

# Catalytic Reactions at Amine-Stabilized and Ligand-Free Platinum Nanoparticles Supported on Titania During Hydrogenation of Alkenes and Aldehydes

Nils Brinkmann<sup>1</sup>, Alexander Damps<sup>1</sup>, Michael Siemer<sup>1</sup>, Jessica Kräuter<sup>1</sup>, Frank Rößner<sup>1</sup>, Katharina Al-Shamery<sup>1</sup>

<sup>1</sup> Institute of Chemistry, Carl von Ossietzky University Oldenburg

## Corresponding Author

Nils Brinkmann

nils.brinkmann@uni-oldenburg.de

## Citation

Brinkmann, N., Damps, A., Siemer, M., Kräuter, J., Rößner, F., Al-Shamery, K. Catalytic Reactions at Amine-Stabilized and Ligand-Free Platinum Nanoparticles Supported on Titania During Hydrogenation of Alkenes and Aldehydes. *J. Vis. Exp.* (184), e63936, doi:10.3791/63936 (2022).

## Date Published

June 24, 2022

## DOI

10.3791/63936

## URL

jove.com/video/63936

## Abstract

Ligands like amines are used in the colloidal synthesis approach to protect platinum nanoparticles (Pt NP's) from agglomeration. Normally, ligands like amines are removed by diverse pre-treatment procedures before use in heterogeneous catalysis as amines are considered as a catalyst poison. However, a possible beneficial influence of these surface modifiers on hydrogenation reactions, which is known from spectator species on metal surfaces, is often neglected.

Therefore, amine-stabilized Pt nanoparticles supported by titania (P25) were used without any pre-treatment in order to elucidate a possible influence of the ligand in liquid phase hydrogenation reactions. The catalytic activity of amine-stabilized Pt nanoparticles of two different sizes was investigated in a double-walled stirring tank reactor at 69 °C to 130 °C and 1 atm hydrogen pressure. The conversion of cyclohexene to cyclohexane was determined by gas chromatography (GC) and was compared to ligand-free Pt particles. All catalysts were checked before and after reaction by transmission electron spectroscopy (TEM) and X-ray photoelectron spectroscopy (XPS) for possible changes in size, shape, and ligand shell. The hydrogenation of cyclohexene in liquid phase revealed a higher conversion for amine-stabilized Pt nanoparticles on titania than the ligand-free particles. The hydrogenation of 5-methylfurfural (5-MF) was chosen for a further test reaction, since the hydrogenation of  $\alpha$ ,  $\beta$ -unsaturated aldehydes is more complex and exhibits various reaction paths. However, XPS and infrared spectroscopy (IR) proved that 5-MF acts as catalyst poison at the given reaction conditions.

## Introduction

Catalysts in the size of a few single atoms up to larger nanoparticles with high surface-to-volume ratios and defined sizes are promising materials for a wide range of heterogeneous catalyzed reactions, such as hydrogenation, dehydrogenation and photocatalytic reactions<sup>1</sup>. Platinum nanoparticles are widely used in industrial processes, due to the high activity for hydrogenation of olefins. Besides, platinum nanoparticles are promising catalysts for the selective hydrogenation of  $\alpha,\beta$ -unsaturated ketones and aldehydes<sup>1,2,3,4</sup>. Here, several parameters such as size, shape, and support are able to affect the catalytic properties<sup>1,5,6</sup>.

The size influences the morphology of nanoparticles, especially in the range of 1 to 5 nm<sup>7</sup>. Specifically, the size influences the available adsorption sites (for instance: edges, steps, or terraces) and thereby the catalytically active surface, which further influences the catalytic activity<sup>7,8,9</sup>. Furthermore, the support is able to interact with the metal. These interactions vary and range from charge transfer or spillover processes to a change in the morphology or encapsulation of nanoparticles<sup>6,10</sup>. While the effect of size, shape, and support on the catalytic properties is well known, a possible effect of adsorbates not directly involved in the reaction, so-called spectator molecules or surface modifiers, is less evolved<sup>1,5,6,11</sup>. In case of a colloidal approach for catalyst preparation, using colloidal metal nanoparticles that are subsequently deposited onto the support, ligands stabilize the nanoparticles and thus may potentially influence the reaction.

The big advantage of the colloidal synthesis is that nanoparticles of a certain size and shape can be produced in a targeted manner helping to control the catalytic performance *via* the synthesis route<sup>12,13,14</sup>. The function of the ligand is to control the size, shape, and morphology of the nanoparticles. However, ligands similar to amines are often considered as catalyst poison, as ligands block available adsorption sites<sup>15,16</sup>. Therefore, to increase the catalytic activity of the catalysts, ligands are commonly removed by pre-treatment, for instance, calcination or UV-light induced decomposition<sup>17,18</sup>.

This stands in contrast to homogeneous catalysis, where ligands are essential for stabilizing the transition metal complexes and tuning their reactivity<sup>15,19</sup>. The interaction between ligand and reactant enables to control the chemoselectivity, regioselectivity, and stereoselectivity of the homogeneously catalyzed reaction. Since the separation of homogenous catalysts from the products is not trivial, heterogeneous catalysts are more common although these are less selective and the question then arises whether ligands also have a positive effect on heterogeneous catalysis.

A promising approach for ligands in heterogeneous catalysis is the use of self-assembling monolayers containing aromatic and aliphatic thiols to improve the selectivity for the hydrogenation of  $\alpha,\beta$ -unsaturated aldehydes and polyunsaturated fatty acids on Pt and Pd nanoparticles. The enhancement of the selectivity is based on several effects. Specific interactions between reactant and modifier, selectively blocking of certain unwanted active sites as well as steric and electronic effects play a role in the selectivity enhancement<sup>20,21,22,23</sup>. A distinction is made between ligands and spectators. Spectators do not participate, but influence the reaction by steric effects, while ligands are involved in reactions<sup>24,25</sup>. A spectator can be formed during a catalytic reaction or by prior chemical processes<sup>11,26</sup>.

The choice of a suitable ligand and solvent for a successful liquid phase hydrogenation is a challenging task. The solvent must have a high solubility for hydrogen as well as for the reactant. Furthermore, there should not be any following or side reactions with the solvent, which can lower the selectivity of the reaction. An appropriate ligand should have a strong adsorption at selected adsorption sites so that the desorption of the ligand under reaction conditions is prevented, but catalytic activity is still present. Ideally, the ligand blocks adsorption sites, which favor side reactions or steer the selectivity of the reaction by the steric demands of the ligand and by interactions with the reactant<sup>15,21</sup>.

This work elucidates whether steric and electronic effects of dodecyl amine (DDA) influence the hydrogenation of cyclohexene and 5-methylfurfural (5-MF) or not. DDA does not interact directly with the reactants, which implies a spectator-directed hydrogenation. 5-MF, a non-toxic derivate of furfural, was used as a more complex and commercially interesting reactant, compared to the hydrogenation of cyclohexene. The selective hydrogenation of furfural, a side product from the production of

bio petroleum, and derivatives of furfural are of industrial interest as these compounds can be gained from the biomass and represent promising starting components for the production of several fine chemicals<sup>27,28</sup>.

However, selective hydrogenation is challenging, since the hydrogenation of the carbon double bonds, and the carbonyl group are competing. Thermodynamically, the hydrogenation of the carbon double bonds is favored against the hydrogenation of the carbonyl group<sup>29</sup>.

## Protocol

### 1. Synthesis of Pt/DDA (1.6 nm) nanoparticles

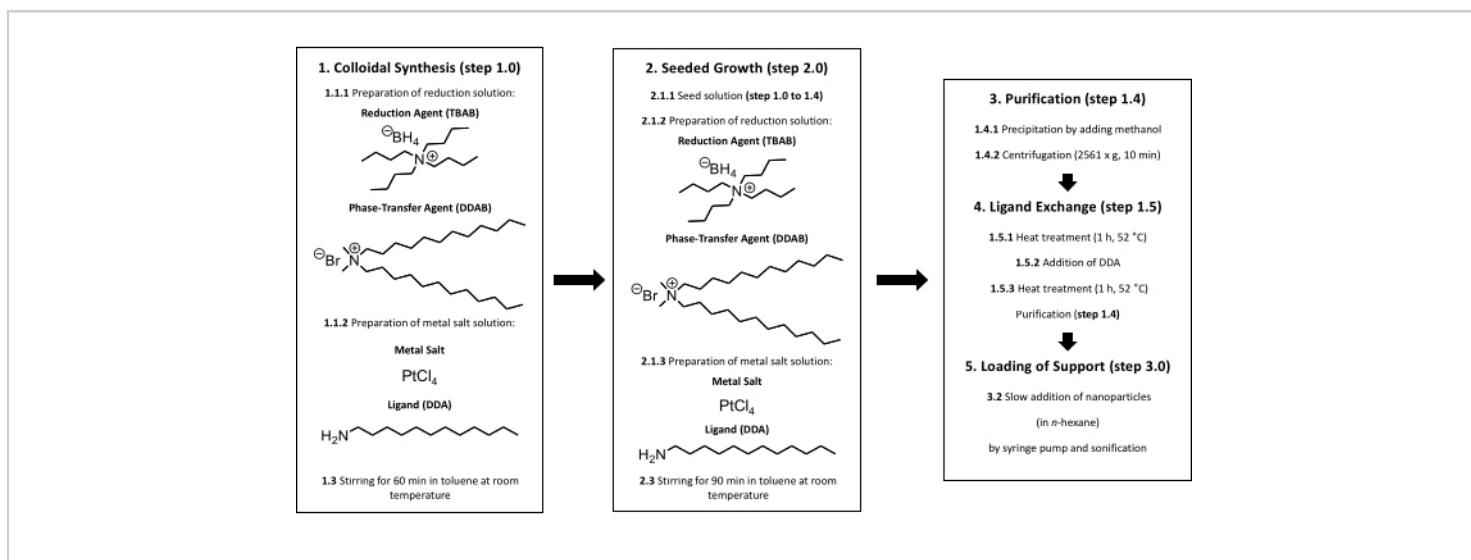


**Figure 1: Colloidal synthesis of supported Pt nanoparticles.** In the beginning, a colloidal synthesis must be performed (step 1). After the addition of the reduction solution to the metal salt solution, the solution is stirred at room temperature for 60 min (step 1.3). From here, two different ways are possible. For gaining bigger nanoparticles, a seeded growth is needed (step 2). After adding the metal salt and reduction solution to the seed solution, the solution is stirred at room temperature for 90 min (step 2.3). After finishing the synthesis (step 1 or step 2), a purification must be done (step 1.4). For avoiding impurities such as halides on the surface a ligand exchange is necessary (step 1.5). The Pt nanoparticles are heated for 60 min at 52 °C in toluene, an additional amount of DDA is added to the solution, and the solution is heated for another 60 min at 52 °C (steps 1.5.1 to 1.5.3). Titania can be loaded with nanoparticles by performing step 3. The particle size is checked by TEM after purification, ligand exchange, and loading of support. [Please click here to view a larger version of this figure.](#)

**NOTE:** The colloidal synthesis approach is shown in **Figure 1** and the experimental steps are described in the following section.

1. Prepare solutions for nanoparticle synthesis

1. For the preparation of the reduction solution dissolve 25.4 mg of the reduction agent tetrabutylammonium borohydride (TBAB) and 46.3 mg of the phase-transfer-agent didodecyldimethylammonium bromide (DDAB) in 1 mL of toluene at room temperature in a 10 mL rolled rim glass.

**CAUTION:** TBAB can lead to cauterization upon contact with the skin. DDAB leads to cauterization upon contact with the skin and is harmful to inhalation. Toluene is slightly flammable and can harm the central nervous system and organs. DDA can lead to cauterization upon contact with the skin and may cause damage to organs if swallowed or if it enters the airways. Therefore, perform the synthesis under the fume hood and wear gloves and goggles.

2. For the preparation of the metal salt solution, dissolve 8.5 mg of the precursor platinum (IV) chloride ( $\text{PtCl}_4$ ) in 2.5 mL of toluene at room temperature in a 10 mL rolled rim glass at first and add 185.4 mg of the ligand dodecyl amine (DDA) after dissolution of  $\text{PtCl}_4$ . Avoid decomposition of hygroscopic chemicals through storage outside the storage container and directly dissolve the chemicals in a solvent. Use only fresh chemicals.

**CAUTION:** DDA is very toxic to aquatic life.  $\text{PtCl}_4$  can lead to cauterization upon contact with the skin and is toxic if swallowed. Therefore, perform the synthesis under the fume hood and wear gloves and goggles. Keep away from possible ignition sources.

Avoid release to the environment. TBAB can lead to cauterization upon contact with the skin. DDAB leads to cauterization upon contact with the skin and is harmful to inhalation.

3. Sonicate both solutions at room temperature for 1-2 min in an ultrasonic bath at a frequency of 35 kHz.  $\text{PtCl}_4$  is sparingly soluble in toluene. The metal salt solution appears slightly yellow after sonification, while the reduction solution is still colorless.

## 2. Starting the reaction

1. Add the complete metal salt solution (1 mL) with a plunge-operated pipette (1,000  $\mu\text{L}$ ) having a disposable tip in a 10 mL round neck flask.

**NOTE:** Mixing phenomena can influence the particle growth.

2. Add the full volume (1 mL) of the reduction solution to the metal salt solution by shock injection to get a narrow size distribution. Use a plunge-operated pipette (1,000  $\mu\text{L}$ ) with a disposable tip while stirring the solution during addition with a magnetic stir bar.

3. Let the reaction solution stir for 60 min under ambient conditions.

**NOTE:** The start of the reaction can be recognized by gas bubbles and a color change of the reaction mixture from yellow to dark gray. The reduction of the Pt precursor and the growth of Pt nanoparticles are fast processes<sup>14</sup>. The solution is stirred for 60 min to ensure that the growth process of the Pt nanoparticles is completed.

## 4. Purification of the nanoparticle solution

1. Purify the Pt nanoparticles by precipitation and centrifugation at room temperature. For this, transfer the complete reaction solution with a plunge-

operated pipette (1,000  $\mu\text{L}$ ) having a disposable tip, into an 80 mL centrifuge tube and add 14 mL of methanol.

**CAUTION:** Methanol is highly flammable and toxic if swallowed or inhaled and in contact with skin. Keep away from possible ignition sources. Add the methanol to the reaction solution under a fume hood while wearing gloves and goggles.

2. Centrifugate at  $2,561 \times g$  for 10 min at room temperature. Dispose the solution after centrifugation.
3. Resolve the nanoparticle residue by adding 3 mL of toluene with a plunge-operated pipette with a disposable tip (1,000  $\mu\text{L}$ ). The nanoparticles should be in the size range of 1.3 nm to 2 nm after this synthesis routine<sup>14</sup>.
4. Transfer the nanoparticle solution from step 1.4.3 into a rolled rim glass (10 mL) for further use.
5. Perform a ligand exchange to remove synthesis residues such as chloride or bromide as described below.
  1. Transfer 3 mL of the purified Pt nanoparticles in toluene into a 100 mL round neck flask and fill with toluene to a final volume of 50 mL. Heat the solution to 52 °C and hold the temperature for 60 min while stirring the solution with a magnetic stir bar.
  2. Solve 185.4 mg of DDA in 2.5 mL of toluene in a 10 mL rolled rim glass at room temperature and add this solution with a plunge operated pipette (1,000  $\mu\text{L}$ ) with a disposable tip to the heat-treated Pt/DDA (1.5 nm) solution at 52 °C.
  3. Heat and stir the solution for further 60 min at 52 °C. Perform a purification as described earlier in step 1.4

but dissolve the Pt nanoparticles in 3 mL of *n*-hexane instead of 3 mL of toluene.

**CAUTION:** *n*-hexane is a highly flammable liquid and vapor. *n*-hexane causes skin irritation and may cause damage to organs if inhaled. *n*-hexane is toxic to aquatic life and suspected to damage fertility. Therefore, perform the synthesis under the fume hood and wear gloves and goggles. Keep away from possible ignition sources. Avoid release to the environment.

**NOTE:** Use *n*-hexane to aid the evaporation of the solvent (see next step).

4. Evaporate the solvent in the fume cupboard overnight at room temperature and ambient pressure and weigh the Pt nanoparticles the next day.

**NOTE:** Weighing the Pt nanoparticles is crucial for determining the amount of titania, which is needed for a defined support loading (see step 3).

## 2. Synthesis of larger Pt nanoparticles (Pt/DDA (2.4 nm)) by a seed-mediated growth process

1. Prepare the solutions for the nanoparticle synthesis.
  1. Dissolve the previously fabricated Pt/DDA (1.6 nm) nanoparticles in 50 mL of toluene in a 100 mL round neck flask at room temperature.
  2. Prepare the reduction solution by dissolving 370.5 mg of DDAB and 200.5 mg of TBAB in 10 mL of toluene at room temperature in a 20 mL rolled rim glass separately.
  3. Dissolve 68.0 mg of PtCl<sub>4</sub> in 10 mL of toluene in a 20 mL rolled rim glass and add 1438.1 mg of DDA subsequently. Use this as a metal

salt solution. Avoid decomposition of hygroscopic chemicals through storage outside the storage container and directly dissolve the chemicals in a solvent.

4. Sonicate both solutions made in steps 2.1.2 and 2.1.3 at room temperature for 1-2 min in the ultrasonic bath at an ultrasonic frequency of 35 kHz.
  5. Draw up both solutions each in a 20 mL disposable syringe with a needle and, if necessary, remove any air in the syringe.
2. To start the reaction, add the additional precursor and reduction solutions from steps 2.1.2 and 2.1.3 very slowly and continuously by using a syringe pump (0.1 mL/min) to the seed solution from step 2.1.1 to prevent the formation of nanowires or a second nucleation<sup>14</sup>. Stir the seed solution at room temperature by using a magnetic stir bar while adding the precursor and reduction solution.
  3. Stir the nanoparticle solution for another 90 min at room temperature after the addition of the reactants. Perform a purification as described in step 1.4 but dissolve the Pt nanoparticles in 3 mL of *n*-hexane instead of 3 mL of toluene. Evaporate the solvent overnight at room temperature and ambient pressure and weigh the Pt nanoparticles the next day.

### 3. Deposition of Pt nanoparticles onto titania (Pt/DDA/P25)

1. Disperse P25 in *n*-hexane (2 mg/mL) at room temperature in an appropriately sized beaker by using an ultrasonic bath at an ultrasonic frequency of 35 kHz.

**NOTE:** The amount of oxide depends on the weight of the dried fabricated nanoparticles.

2. Prepare a nanoparticle solution of the previously fabricated particles (1 mg/mL in *n*-hexane) and add this solution to the dispersed P25 at room temperature using a disposable syringe (20 mL) with needle at a flow rate of 0.016 mL/min by using a syringe pump.

**NOTE:** The adsorption of nanoparticles on the oxide becomes visible by a color change of the solution from gray to colorless.

3. Dry the loaded powder under ambient conditions overnight in the fume cupboard and subsequently for 10 min in vacuum (0.01 mbar).

#### 4. Synthesis of amine-free titania supported Pt nanoparticles by impregnation

1. Fill 1,000 mg of titania (P25) in a crystallizing dish (50 mL) and add water until P25 is covered.
2. Dissolve 3 g of chloroplatinic acid hexahydrate ( $\text{H}_2\text{PtCl}_6 \cdot 6 \text{H}_2\text{O}$ ) in 20 mL of distilled water and add the aqueous solution to the submitted P25 with a 20 mL volumetric pipette.

**CAUTION:** Chloroplatinic acid hexahydrate can lead to cauterization when in contact with the skin and is toxic if swallowed. Therefore, perform the synthesis under the fume hood and wear gloves and goggles.

**NOTE:** The amount of chloroplatinic acid varies depending on the desired nanoparticle loadings of the oxidic support.

3. Heat and maintain the solution at 75 °C while stirring with a magnetic stir bar for 4 h until the solution is viscous. Dry the solution in the crystallizing dish for 1 d at 130 °C in an oven under atmospheric conditions.
4. Perform a calcination in a temperature-programmed oven under atmospheric conditions. Fill the powder from

step 4.3 in a porcelain crucible. Heat up to 400 °C within 30 min and hold the temperature for 4 h. Cool the sample down to room temperature without using a temperature ramp.

5. Perform a reduction of the catalyst in a tube furnace. Heat to 180 °C with a temperature ramp of 4 °C/min and hold the temperature for 1.5 h under a continuous flow of hydrogen. Check for a continuous hydrogen flow with a bubble counter.

## 5. Liquid phase hydrogenations

1. Prepare the double-walled reactor for the catalytic measurements.
  1. Fill the heating jacket with the desired heating medium. Use diisopropyl ether for an operating temperature of 69 °C in the reactor.

**NOTE:** A list of other used heating media can be found in the supplementary files (see **Supplementary Table S1**).
  2. Fill the stirred tank reactor with 120 mL of toluene and the synthesized catalyst (1 mg/mL). Degas the stirring tank reactor by applying a vacuum of around 360 mbar.
  3. Remove oxygen by purging. Put a rubber balloon, filled with 1 atm hydrogen, on top of the reflux condenser and flush the stirring tank reactor with hydrogen. Repeat the purging process five times.
  4. Start heating and stirring the reactor tank with a magnetic stir bar under hydrogen atmosphere.

2. Start the catalytic reaction

**NOTE:** Before a catalytic test was carried out, possible hydrogenation of the solvent under the reaction conditions was checked, but this was not the case (see

**Supplementary Figure S1** and **Supplementary Table S2**). The gas chromatogram in **Supplementary Figure S1** shows additional peaks, which can be assigned to contaminations in toluene, as they are also present in a sample of toluene taken from the storage container (see **Supplementary Figure S2** and **Supplementary Table S3**).

1. Inject the reactant, in this case, 1 mL of cyclohexene, with a disposable syringe with a needle *via* the rubber septum with a specific thermal and solvent stability after reaching a constant temperature. Take 1 mL samples using a disposable syringe every 10 min.
2. Use a syringe filter (pore size: 0.2  $\mu\text{m}$ ) to separate the catalyst from the reaction solution and fill the liquid into an autosampler vial that is sealed properly afterward.

**NOTE:** Instead of a syringe filter, centrifugation is also possible to remove the catalyst.

**CAUTION:** Cyclohexene is a highly flammable liquid and vapor. Cyclohexene is harmful if swallowed and toxic when it comes in contact with the skin. Therefore, perform the synthesis under the fume hood and wear gloves and goggles.

3. Test the poisoning effect of 5-methylfurfural. Prepare the stirring tank reactor as described in step 5.1.

**NOTE:** 5-MF does not show any conversion on the supported Pt catalysts (see **Supplementary Table S4** and **Supplementary Figure S3**). Whether a poisoning effect occurs, can be checked by adding 5-MF to the hydrogenation reaction of cyclohexene.

4. For testing the poisoning effect of 5-MF on the Pt nanoparticles proceed as follows: first, inject 5-MF (5 mmol) to the submitted catalyst in toluene and let the mixture stir for 120 min.
  5. Add cyclohexene with a disposable syringe in a molar ratio of 1:1 and 1:10 to 5-MF. For determining the reaction process, take 1 mL samples using a disposable syringe with a needle every 10 min.
  6. Use a syringe filter (pore size: 0.2  $\mu\text{m}$ ) to separate the catalyst from the reaction solution and fill the liquid into an autosampler vial that is sealed properly afterward.  
**NOTE:** Instead of a syringe filter, centrifugation could also be done to remove the catalyst.
3. Analyze the products by GC. Use a column with the following specifications: length = 50 m, film = dimethylpolysiloxane, film thickness = 0.5  $\mu\text{m}$ , inner diameter = 0.2 mm. Apply an injector temperature of 200  $^{\circ}\text{C}$  with a split ratio of 40:1.
  4. Start with a column temperature of 40  $^{\circ}\text{C}$  and hold the temperature for 6 min. Heat from 40  $^{\circ}\text{C}$  to 180  $^{\circ}\text{C}$  with a temperature ramp of 15  $^{\circ}\text{C}/\text{min}$ . Measure with a hydrogen flow of 0.6 mL/min and a temperature of 300  $^{\circ}\text{C}$  for the FID detector.
    1. Inject the samples into the GC. Assign the peaks to the different substances by comparison with reference standards (see **Supplementary Table S5** and **Supplementary Figure S4**).
    2. Evaluate the gas chromatograms using the 100% method. Calculate the percentage amount of each compound by dividing the measured peak area for this compound by the sum of all peak areas.

## 6. Preparation for TEM measurements

1. Load the samples onto a 300-mesh copper grid coated with formvar and coal.
  1. For loading the grid with bare Pt nanoparticles, extract 0.1 mL of the purified Pt nanoparticle solution in *n*-hexane and dilute the extracted solution by adding 2 mL of *n*-hexane in a rolled rim glass (10 mL). Transfer 8.5  $\mu$ L of the diluted solution on the grid with a plunge-operated pipette (10  $\mu$ L) with a disposable tip and let the grid dry overnight at room temperature at ambient pressure.
  2. For loading the grid with powders, dip the grid very carefully into the powder to prevent the grid from any damage and remove excess powder by an air stream created by a Pasteur pipette (length: 145 mm, inside diameter: 1.5 mm) with a pipette ball (diameter: 94 mm).
2. Place the grid in a TEM cartridge sample holder. Introduce the sample holder into the TEM column. Follow the standard operating procedure for handling the transmission electron microscope.
3. Take pictures at an acceleration voltage of 80 keV with a magnification of 250,000 and import the pictures to an image editing software.
4. Determine the nanoparticle silhouette by the contrast threshold of the images, for analysis of the pictures with the image editing software. The image analysis software assumes a spherical outline of the particles.
5. Remove overlaid particles and particles lying at the edges of the image, which can falsify the particle size distribution, by erasing these particles with the software's built-in drawing tools. To identify superimposed particles,

compare the processed image (step 6.4) with the original image.

6. Use the built-in software tools for the analysis of the particle size. Measure the size of the supported Pt nanoparticles manually with the software built-in tools. Analyze supported Pt nanoparticles manually since the low contrast difference between nanoparticles and support allows no automatic analysis by the software.

## 7. XPS measurements of synthesized samples

1. Prepare a silicon wafer for the XPS measurements of bare nanoparticles by immersing the wafer in a rolled rim glass (10 mL) filled with acetone and sonicate the wafer for 1 min at a frequency of 35 kHz. Repeat the procedure with 2-propanol.
2. Coat the cleaned and dried silicon wafer fragment with a concentrated solution of purified Pt nanoparticles in *n*-hexane by drop casting with a micropipette. Dry the wafer overnight at room temperature and ambient pressure under a fume hood. Attach the specimen to the sample holder by using carbon tape.  
**NOTE:** The droplet size was not determined, nor was any specific droplet size placed on the wafers. The volume of the solution drawn up in the micropipette was selected so that the drop cannot overflow. Uniform wetting of the wafers or KBr pellets (see step 8.3) is difficult due to the drying effects of the solvent.
3. Prepare a pit sample holder for powders by immersing the sample holder in a rolled rim glass (10 mL) with acetone and sonicate the sample holder for 1 min at an ultrasonic frequency of 35 kHz. Repeat the procedure with 2-propanol.

4. Fill the sample into the pit of the cleaned and dried sample holder. Place a clean cling film between stamp and sample to avoid contaminations and press the sample using the stamp.
5. To identify a possible poisoning effect by 5-MF after hydrogenation, prepare a Pt film covered with 5-MF as a reference sample.
  1. Clean a silicon wafer part by immersing the wafer in a rolled rim glass (10 mL) with acetone and sonicate the wafer for 1 min (ultrasonic frequency: 35 kHz). Repeat the procedure with 2-propanol. Coat the cleaned silicon wafer with a 10 nm Pt film by using an argon-assisted Pt sputter system. For operating the sputtering system follows standard procedures provided in the user manual.
  2. Dissolve 1 mmol of 5-MF in 2.5 mL of toluene in a rolled rim glass (10 mL). Wet the Pt film with 5-MF by drop casting with a micropipette and dry the sample overnight at room temperature and ambient pressure under a fume hood.
6. Introduce the sample into the XPS analysis chamber. Start the measurement using the following parameters: radiation source: Al E(K $\alpha$ ) = 1486.8 eV (monochromatic), spot size: 650  $\mu$ m, pass energy: 40 eV, dwell time: 100 ms, energy step size: 0.05 eV, number of scans: 10 for Pt4f- and N1s-detailed spectra; 5 for C1s and O1s detailed spectra, charge compensation by Ar flood gun.
7. After finishing the measurements, load the spectra into a software with built-in tools for applying a background and fitting the different signals. Fit the signals with a Shirley background and Gaussian-Lorentzian curves with a Gauss Lorentz ratio of 30. Add a tailing to the Gaussian-Lorentzian curves for metallic platinum

signals. Reference all the measured signals to the measured adventitious C1s-signal at 284.8 eV for compensating charging effects<sup>30</sup>.

## 8. FT-IR measurements

1. Prepare Pt/DDA (1.6 nm) and Pt/5-MF nanoparticles for the FT-IR measurements. For the synthesis of Pt/5-MF nanoparticles perform a synthesis with ligand exchange with 5-MF instead of DDA (steps 1.0 to 1.5.3). For purification of the Pt/5-MF nanoparticles after ligand exchange use *n*-hexane instead of methanol for precipitation of the Pt nanoparticles. Resolve the purified Pt nanoparticles in 1 mL of methanol.
2. Prepare potassium bromide (KBr) pellets of approximately 1 mm thickness by using a hydraulic press. Pestle KBr, which was stored in water-free conditions, before filling in the press. Press the pellets with a pressure of 10 bar for 15 min.
3. Coat the KBr pellets by drop casting with the solution of the purified Pt nanoparticles multiple times by using a micropipette. Let the pellet dry between each drop to avoid liquid trickling over the edges of the pellet. Dry the KBr pellet at room temperature and ambient pressure for 2 h under a fume hood.
4. Perform the FT-IR measurements.
  1. For measuring a background, place an uncoated KBr pellet in the IR sample holder. Use a resolution of  $1\text{ cm}^{-1}$  and a measurement time of 60 min.
  2. Place a loaded KBr pellet in the sample holder and use the same parameters as described in step 8.4.1.

3. Use the built-in software tools to subtract the background spectra from the sample spectra and perform a manual baseline correction.
5. Use a quantum chemistry *ab initio* program for frequency calculations of vibrational modes. Perform the calculations using the density functional *PBE0* and the basic set *6-311G\**. Use the theoretical calculations as a rough guide for the assignment of absorption bands.

## Representative Results

The results of the synthesis and catalytic testing of different Pt nanoparticles are presented here. First, the

synthesized Pt nanoparticles as well as the particles supported on P25 were characterized by TEM for their shape and size. Furthermore, their chemical composition, e.g., oxidation states of the different elements and their chemical environment was investigated by XPS. Afterwards, the supported Pt nanoparticles were checked for their catalytic performance for the hydrogenation of alkenes, cyclohexene was used here, and aldehydes such as 5-MF. As the hydrogenation of aldehydes does not show any conversion under the used reaction conditions further systematical studies were done to elucidate a possible surface poisoning of the Pt nanoparticles.

### **Characterization of the catalysts**

The particle size and shape of the Pt nanoparticles as well as the particles supported on P25 were checked by TEM, since the particle size and shape can influence the catalytic activity<sup>31</sup>. The TEM images in **Figure 2** reveal that the Pt nanoparticles exhibit a quasi-spherical shape directly after colloidal synthesis (**Figure 2A**). The size and shape remain the same after ligand exchange with DDA (**Figure**

**2B**). However, bigger particles (**Figure 2C**), synthesized by crystal growth, are more asymmetrical in shape and show partly tripodal and ellipsoidal shapes. After deposition of Pt/DDA (1.6 nm) on titania (**Figure 2B**) no change in size and shape occurred (**Figure 2D**). The size and shape of the amine-free platinum catalyst Pt/P25 (2.1 nm), synthesized by impregnation (**Figure 2E**) is in the same range compared to the platinum nanoparticles, synthesized by the colloidal synthesis.

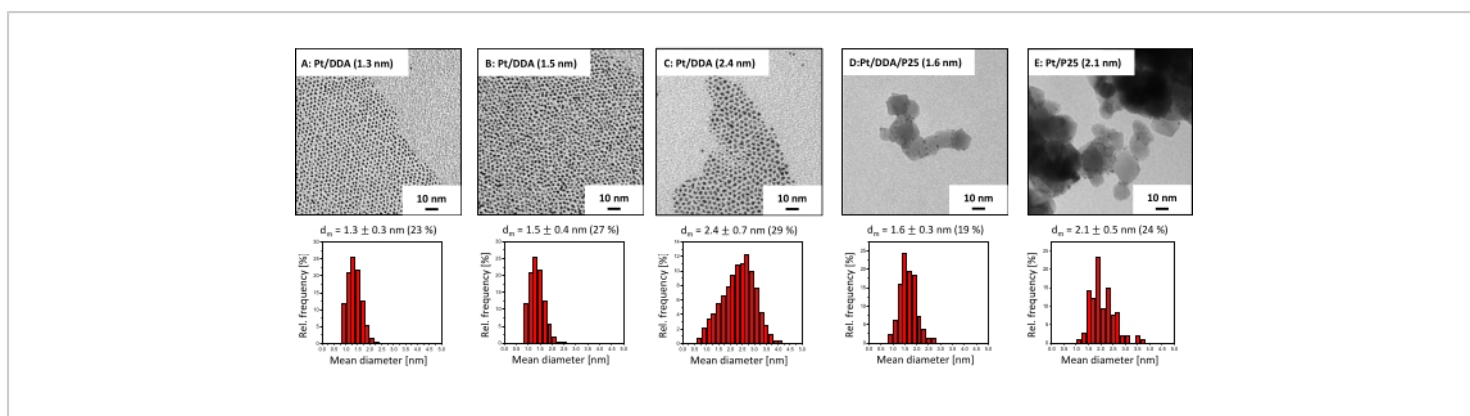


**Figure 2: TEM images and size histograms of amine-stabilized platinum nanoparticles and titania supported platinum catalysts.** Shown are the TEM images (at the top) and the size histograms (at the bottom) of **(A)** as-synthesized (Pt/DDA (1.3 nm)), **(B)** after ligand exchange with DDA (Pt/DDA (1.5 nm)), **(C)** after seeded growth (Pt/DDA (2.4 nm)), **(D)** after deposition on titania (Pt/DDA/P25 (1.6 nm)), and **(E)** amine-free platinum nanoparticles supported on titania (Pt/P25 (2.1 nm)). TEM images were recorded using an acceleration voltage of 80 eV. [Please click here to view a larger version of this figure.](#)

XPS was used to get chemical information on the surface adsorbate species. The Pt nanoparticles before and after ligand exchange were characterized as well as Pt nanoparticles after deposition on titania and the amine-free Pt nanoparticles. The XP spectra are shown in **Figure 3**. The Pt4f spectrum of Pt/DDA nanoparticles (1.3 nm) shall be discussed first (**Figure 3**, top spectrum). The Pt4f spectrum shows two signals at 71.5 eV and 74.8 eV due to spin-orbit splitting, which have a specific area ratio of 4:3. The Pt4f<sub>7/2</sub>

signal at 71.5 eV can be assigned to Pt nanoparticles (1.3 nm) and is shifted upward by 0.4 eV compared to 71.1 eV for bulk Pt<sup>32</sup>. However, the measured binding energy agrees well with Pt/DDA nanoparticles (1.3 nm) on a gold film<sup>33</sup>. The difference in the binding energy between the bulk Pt and the small Pt/DDA nanoparticles can be explained by a size effect. Slight shifts of the Pt signal by 0.2 eV after ligand exchange without change in the size of the platinum particles lies within

the measurement precision for the binding energy. While no difference can be observed after deposition on titania, the XP spectra of Pt/P25 (2.1 nm) synthesized by the impregnation method show a down-shift of the Pt4f<sub>7/2</sub> peak by 0.6 eV compared to Pt/DDA/P25 (1.6 nm) and a down-shift of 0.2 eV compared to bulk Pt<sup>32</sup>. Additional species are observed at higher binding energies, which can be attributed to oxidized Pt<sup>2+</sup> and Pt<sup>4+</sup> species<sup>34</sup>. The Pt4f<sub>5/2</sub> peak of Pt<sup>0</sup> and the Pt4f<sub>7/2</sub> peak of Pt<sup>4+</sup> have a similar binding energy with 74.2 eV and 75.0 eV and therefore overlap each other.

In the C1s region, three signals arise between 289.0 eV and 284.0 eV in all shown spectra. All XP spectra are referenced to adventitious carbon at 284.8 eV<sup>30</sup>. The assignment of the signals to different carbon species is difficult. The alpha carbon of the amine is expected to arise at 285.4 eV and 285.6 eV<sup>35,36</sup>. However, the signal can shift due to charging effects, so that the signal can be superimposed with carbon atoms in the vicinity to oxygen. The signals between 286.3 eV and 289.0 eV can be assigned to carbon bonded to oxygen<sup>37</sup>. Possibly, a contamination with carbon dioxide or an undergoing surface reaction of the ligands leads to the formation of both carbon species<sup>38</sup>.

The N1s detailed spectrum of the as-prepared small Pt nanoparticles (**Figure 3**, top spectrum) exhibits three different nitrogen species at 402.6 eV, 399.9 eV, and 398.2 eV. The signal at 402.6 eV can be assigned to an ammonium compound<sup>39</sup>, while the signal at 399.9 eV corresponds to the adsorbed amine ligand<sup>33</sup>. The presence of bromide (Br3d<sub>5/2</sub> at 68.2 eV) in the Pt4f spectra and the ammonium

species in the N1s detailed spectra are due to the use of DDAB as phase-transfer-agent. However, a formation by moisture or autooxidation of the amine cannot be excluded here<sup>35</sup>. The additional species at 398.2 eV is shifted to lower binding energies in comparison to the amine signal and possibly appears according to an amine-surface-interaction. Several species, for instance oligomers and amides have been assigned to that signal<sup>35,40</sup>. Furthermore, amines can undergo deprotonation reactions on Pt(111) surfaces, which can be the reason for the additional species<sup>41,42</sup>. By performing a ligand exchange, the ammonium compound can be removed, while the additional amine-surface species is still present on the platinum surface. Interestingly, the amine signal shows almost the same binding energy as observed for the Pt nanoparticles before ligand exchange, while the additional species is shifted by 0.3 eV to lower binding energies after deposition on titania. The position of the additional amine surface species can be explained by a stronger interaction with the surface which may occur in two scenarios. On the one hand, amine could be still present after deposition on P25, but not in direct contact with the Pt surface. On the other hand, the support already revealed a signal at this position in the N1s detail spectrum, which can be related to impurities (see **Supplementary Figure S5**). These most likely result from the P25 production or the used cleaning procedure in industry<sup>43</sup>, although a contamination by residues in the analysis chamber of the spectrometer or from the atmosphere cannot be fully excluded here. This also explains the presence of amine for the ligand-free Pt/P25 (2.1 nm).

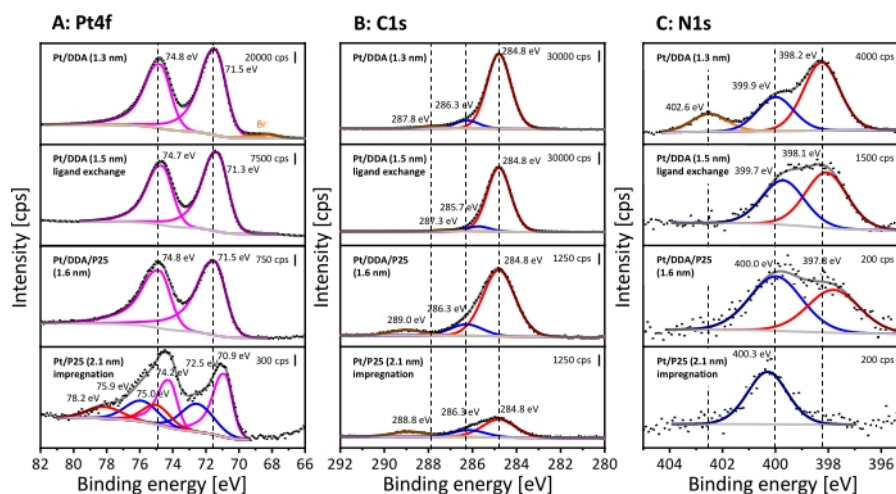


**Figure 3: XPS analysis of colloidal Pt/DDA nanoparticles and titania supported catalysts.** Shown are the Pt4f detailed spectra (A), the C1s detailed spectra (B) and the N1s detailed spectra (C). The stacked XP spectra represent Pt/DDA (1.3 nm) before ligand exchange (shown at the top), Pt/DDA (1.5 nm) after ligand exchange (below), Pt/DDA/P25 (1.6 nm) after deposition on titania and Pt/P25 (2.1 nm) synthesized by impregnation (shown at the bottom). The dotted lines show the measured intensity, the light gray lines show the subtracted background, and the dark gray lines show the sum of all fitted species. The colored lines show the single fitted species. The Pt4f detailed spectra reveal metallic Pt4f<sub>7/2</sub> and Pt4f<sub>5/2</sub> (magenta) and oxidized Pt<sup>2+</sup> (blue) and Pt<sup>4+</sup> (red) species. The orange lines show the presence of bromide (Br<sup>-</sup> 3d<sub>5/2</sub> and Br<sup>-</sup> 3d<sub>3/2</sub>). Three different carbon species are present in the C1s detailed spectra, which are colored red, blue, and orange. However, an assignment to individual species is difficult. The N1s detailed spectra reveal ammonium (orange), amine (blue), and an additional amine-surface species (red). The spectra were measured with Al K $\alpha$  (monochromatic) radiation source (pass energy: 40 eV, energy step size: 0.05 eV, and number of scans: 10) and were referenced on the aliphatic C1s signal at 284.8 eV<sup>30</sup>. [Please click here to view a larger version of this figure.](#)

### Catalytic testing

After characterization with TEM and XPS, the hydrogenation performance of titania-supported Pt nanoparticles was tested by regarding the cyclohexene hydrogenation as the model reaction. The comparison with nanoparticles synthesized by impregnation should elucidate a possible influence of the ligands on the hydrogenation. For that, the reaction was carried out in a double-walled stirring tank reactor under hydrogen atmosphere. Toluene, which was used as a

solvent, was not hydrogenated under reaction conditions (see **Supplementary Figure S1**). **Figure 4** shows the conversion of cyclohexene dependent on the reaction time for Pt/DDA/P25 before (1.3 nm) and after ligand exchange (1.6 nm), for bigger particles Pt/DDA/P25 (2.4 nm) and amine-free Pt/P25 (2.1 nm).

The as-synthesized Pt/DDA/P25 catalyst (1.3 nm) without ligand exchange procedure (step 1.5) exhibits a conversion

of cyclohexene up to 56% after a reaction time of 60 min, while the Pt/DDA particles (1.6 nm) on which a ligand exchange was performed, convert cyclohexene up to 72% after the same reaction time. The ligand-free particles show a noticeably lower conversion of 35% compared to the amine-stabilized particles under the same conditions. This result is very promising since the amine-free catalyst does not exhibit any ligands, which could partially block the platinum surface except for adsorbed solvent. The different activities of the catalysts shall be discussed later. In addition, larger amine-stabilized Pt/DDA nanoparticles (2.4 nm) on titania, synthesized by crystal growth<sup>14</sup> were also tested and compared with smaller Pt/DDA particles on titania (1.6 nm)

with identical weight loading (0.1 wt%). The conversion of cyclohexene over the smaller Pt/DDA particles (1.6 nm) by 72% is slightly better than the conversion over the bigger Pt/DDA particles (2.4 nm) by 67%. Here, no significant size effect could be observed for the hydrogenation of cyclohexene over the amine-stabilized Pt nanoparticles (1.6 nm and 2.4 nm). This result is in accordance with results from literature for the hydrogenation of cyclohexene over ligand-free Pt nanoparticles of different sizes, indicating, that the hydrogenation of cyclohexene is not size dependent<sup>44</sup>. Since the small Pt particles on titania (1.6 nm) showed the best results, these particles were taken into account for further experiments.

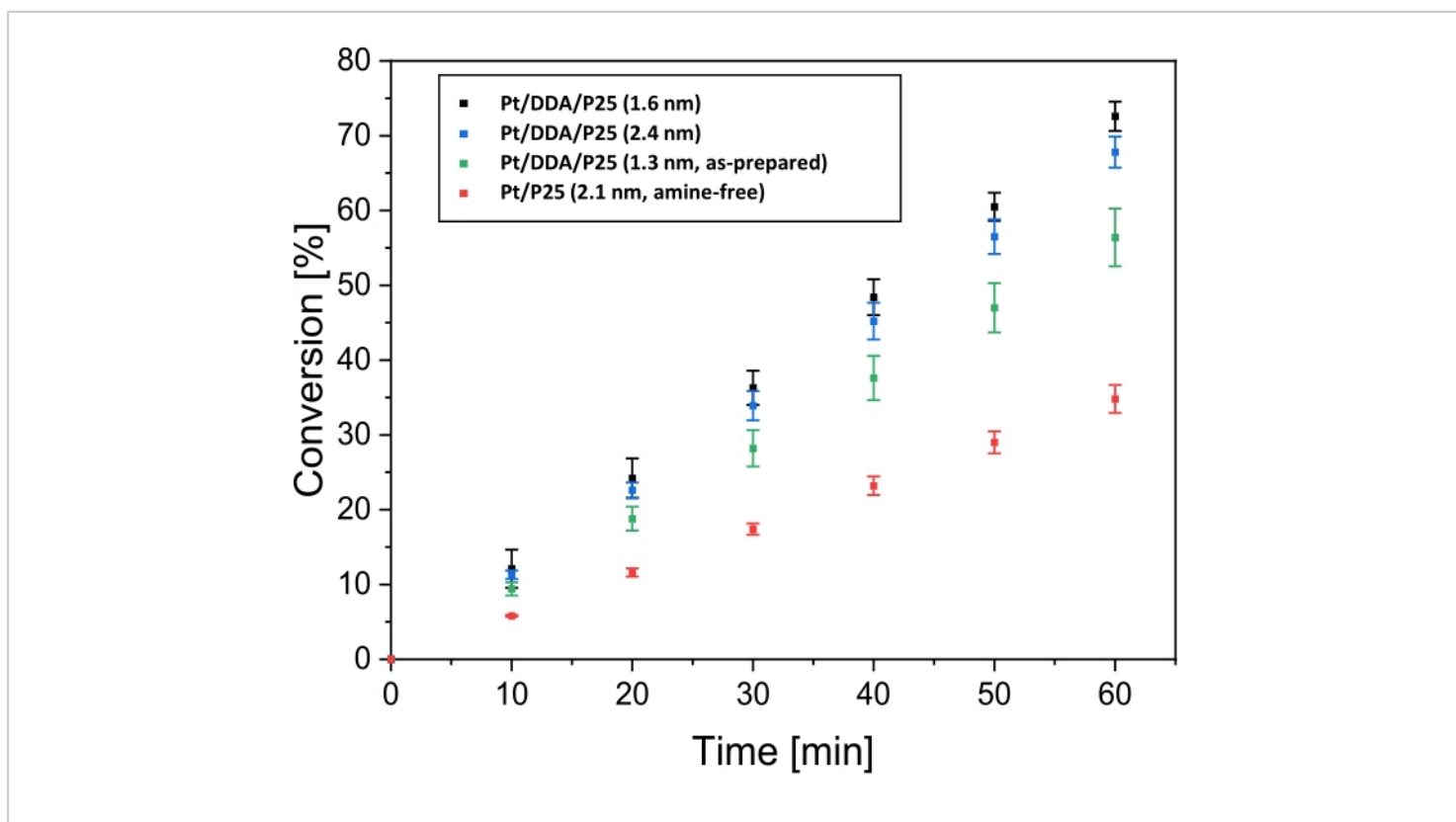


**Figure 4: Conversion over time for the hydrogenation of cyclohexene over titania supported platinum catalysts.**

Shown are the conversion over time plots for the hydrogenation of cyclohexene at 69 °C and 1 bar hydrogen pressure in toluene over Pt/DDA/P25 (1.6 nm; black dots), over Pt/DDA/P25 (2.4 nm; blue dots), over Pt/DDA/P25 as-synthesized (1.3

nm; green dots) and amine-free Pt/P25 (2.1 nm; red dots). The hydrogenation was carried out in a double-walled stirring tank reactor. Error bars represent the calculated standard error. Each measurement series was carried out three times. [Please click here to view a larger version of this figure.](#)

The successful hydrogenation of cyclohexene shows that the solubility of hydrogen in toluene is sufficient under the reaction conditions for the examination of liquid phase hydrogenations.

After testing the catalytic activity of the Pt catalysts for the hydrogenation of cyclohexene, the hydrogenation of 5-MF was also investigated, since 5-MF is a derivate of furfural, which can be gained from biomass and is a promising starting material for the production of several fine chemicals<sup>27</sup>. The amine-stabilized and amine-free Pt nanoparticles were tested at a reaction temperature range from 70 °C to 130 °C. Besides toluene, 2-propanol was also used as solvent. Furthermore, the hydrogenation was performed under solvent-free conditions. However, no conversion has been observed for any of the catalysts under these conditions.

### Checking for substrate inhibition

As no conversion of 5-MF in liquid phase could be seen in the gas chromatogram (see **Supplementary Figure S3**), further investigations on the influence of 5-MF on the cyclohexene

conversion were performed. These experiments were done to reveal whether 5-MF or a surface species of 5-MF as well as possible reaction products act as catalyst poison under these conditions. Previously, Pt/DDA/P25 (1.6 nm) exhibited the highest conversion, that is why this catalyst was used in this reaction. The conversion of cyclohexene with an increasing amount of 5-MF dependent on the reaction time is presented in **Figure 5**.

As already shown in the previous chapter, the conversion of cyclohexene was 72% after 60 min reaction time and in the absence of 5-MF. After adding the same amount of 5-MF the conversion rate of cyclohexene decreases to 30%. A higher amount of 5-MF in the ratio of 10:1 with respect to cyclohexene leads to a further decrease in the conversion, down to 21%. As a conclusion, a blocking of the active surface sites by 5-MF becomes more likely. This would correspond to an inhibition of the titania supported Pt nanoparticles by the reactant. However, hydrogenation is still possible with an excess of 5-MF.

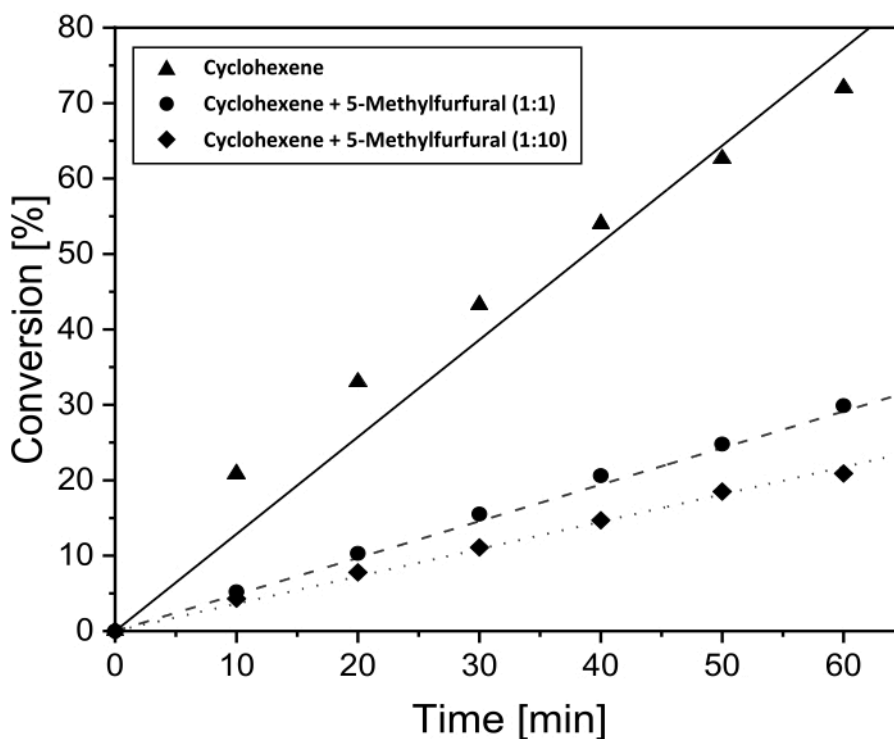


**Figure 5: Conversion over time for the hydrogenation of cyclohexene with addition of 5-MF for proof of poisoning effects.** Conversion over time plots for the hydrogenation of cyclohexene over Pt/DDA/P25 (1.6 nm) without addition of 5-MF (solid line) and with addition of 5-MF in the volume ratio of 1:1 (dashed line) and 1:10 (dotted line) to the cyclohexene. The hydrogenation was performed at 69 °C and 1 bar hydrogen pressure in toluene using a double-walled stirring tank reactor.

[Please click here to view a larger version of this figure.](#)

To prove that, the catalyst was analyzed by TEM and XPS before and after the reaction, as described before. Since TEM images do not reveal any changes, only the XP spectra shall be discussed in the following (for TEM images see **Supplementary Figure S6**). The measured XP spectra are shown in **Figure 6**. The spectra will be compared with 5-MF adsorbed on a Pt film to distinguish between a poisoning by 5-MF or a reaction species.

Here only the most important things are summed up, as the XP spectra of the catalyst before usage were discussed above. The Pt4f detailed spectrum reveals two signals

appearing at 74.8 eV (Pt4f<sub>5/2</sub>) and at 71.5 eV (Pt4f<sub>7/2</sub>). Both can be assigned to the Pt nanoparticles. As mentioned earlier, the assignment of the species in the C1s spectrum can be difficult due to charging effects, which can lead to overlapping signals of the alpha carbon and carbon atoms in the vicinity of oxygen. However, structural changes in the ligand shell, for instance, a replacement of DDA, should lead to changes in the relative intensities between the signals. Furthermore, the N1s region also shows two signals corresponding to amine (400.0 eV) and a further surface species (397.8 eV).

After the reaction, many changes can be observed in XPS although TEM does not reveal any changes in form and size of the particles. The Pt signals are shifted by 0.6 eV to lower binding energies after hydrogenation. The C1s detailed spectrum reveals the same three signals as already discussed. However, the signal at 289.0 eV shifts by 0.7 eV to lower binding energies in contrast to the unused catalyst. All spectra are referenced to the signal at 284.8 eV. One should note that the ratio between the adventitious carbon and the higher binding energy species changes from 1:0.2:0.1 to 1:0.4:0.3 after hydrogenation. Thus, the relative amount of carbon atoms in vicinity to oxygen raises, which indicates that 5-methylfurfural may adsorb on the platinum surface.

While no shift is visible in the N1s detailed spectra, the amount of nitrogen decreases after usage. Based on the C1s, N1s, and the Pt4f signals the nitrogen/carbon and nitrogen/platinum ratio was determined. The carbon/nitrogen ratio increases from 13:1 to 27:1 while the nitrogen/platinum ratio shows a decrease by a similar factor from 1.2:1 to 0.6:1 after hydrogenation. This may be caused by a partial exchange of the DDA with 5-MF and further indicates a blocking of the surface by 5-MF.

The downshift of the Pt signals after reaction can be explained by an increasing charge density at the Pt nanoparticles. Possibly, metal-support interactions can occur under reaction

conditions, which may lead to a down-shift by an electron transfer from the support towards the metal<sup>45,46,47</sup>. Another possibility is that adsorbed 5-MF could cause a down-shift due to a donor effect. However, the Pt film covered with 5-MF shows the opposite behavior in the Pt 4f signal. Here, the signals are shifted by 0.8 eV to higher binding energies compared to the synthesized Pt/DDA/P25 (1.6 nm). The hydrogen adsorption on platinum also may lead to changes in the binding energy of the Pt4f signal, as has already been demonstrated for a Pt(111) surface by ambient pressure XPS measurements<sup>48</sup>. The shift for the single crystal is 0.4 eV. Here, a downshift by 0.7 eV is observed. A possible explanation is that the particles are more sensitive than the bulk material to electronic changes and the whole particle may be fully saturated with hydrogen. The shift of the carbon species from 289.0 eV to 288.3 eV after exposure to 5-MF indicates the presence of a new carbon species containing a carbon-oxygen bond. Since the Pt film covered by 5-MF shows the same species, this signal can be attributed to the aldehyde group of 5-MF. However, the species at 286.3 eV before and after the use of the catalyst is shifted up by 0.5 eV compared to the carbon species at 285.8 eV of the 5-MF on a Pt film. Charging effects as well as the film thickness of the 5-MF film can lead to a change in the binding energy, so, as already mentioned, a discussion of this species is difficult.

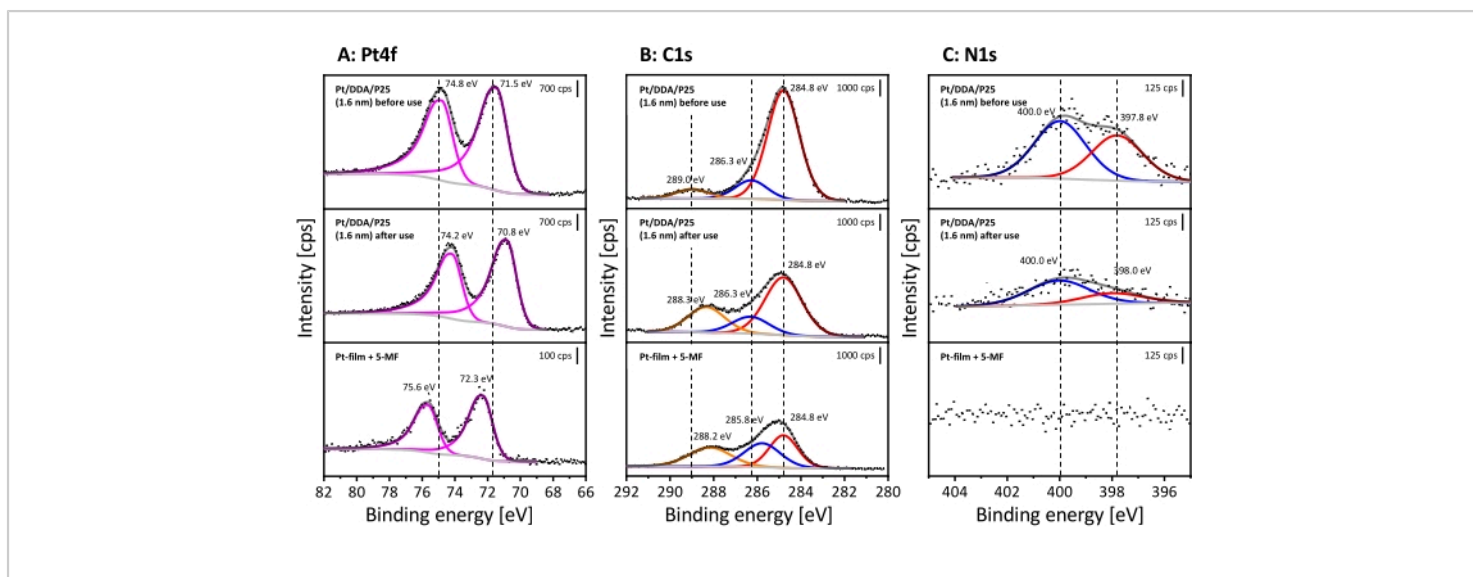


**Figure 6: Proof of surface poisoning after the hydrogenation of 5-MF in liquid phase using XPS.** Shown are the detailed spectra of the Pt4f signal (A), C1s signal (B) and N1s signal (C). The stacked XP spectra represent Pt/DDA/P25 (1.6 nm) before use (on the top) and after hydrogenation of pure 5-MF (in the middle). For comparison, a Pt film covered with 5-MF is shown at the bottom. All spectra were measured with Al K $\alpha$  (monochromatic) radiation source (pass energy: 40 eV, energy step size: 0.05 eV and number of scans: 10). All spectra are referenced on the aliphatic C1s signal at 284.8 eV<sup>30</sup>. [Please click here to view a larger version of this figure.](#)

To gain further insights into the poisoning effect and to distinguish between a poisoning by 5-MF and possible surface species, Fourier-transform-infrared (FT-IR) spectroscopy was performed. Here, FT-IR spectra of Pt nanoparticles before and after adding 5-MF to the catalyst were compared with pure DDA and 5-MF as reference. To assign the arising bands a comparison with theoretical calculations and experiments from literature was performed. The measured FT-IR spectra in the region of 3500 cm<sup>-1</sup> to 700 cm<sup>-1</sup> are shown in **Figure 7**. All observed bands are additionally listed with an assignment to a vibration mode in **Supplementary Table S6** and **Supplementary Table S7**.

The region between 2,500 cm<sup>-1</sup> and 1,300 cm<sup>-1</sup> was not considered, as numerous strongly overlapping absorption bands of water and carbon dioxide from the atmosphere

clog this region. Unfortunately, this region also exhibits some analytically useful absorption bands, such as the carbonyl valence vibration band of an aromatic aldehyde, which is expected to arise between 1715 cm<sup>-1</sup> and 1695 cm<sup>-1</sup><sup>49,50</sup>. First, the specific bands and their assignment to the corresponding molecular vibrations of DDA and 5-MF shall be discussed. Afterwards, these spectra will be compared with the measured FT-IR spectra of the Pt nanoparticles before and after getting in touch with 5-MF. The ligand DDA shows strong bands in the range from 2,851 cm<sup>-1</sup> to 2,954 cm<sup>-1</sup> that can be assigned to the symmetric and asymmetric stretch vibrations of the methyl and methylene groups. The intense and sharp band at 3331 cm<sup>-1</sup> results from the N-H stretch vibration of the amine group<sup>49,51</sup>. This band can be taken to monitor the binding situation

of DDA on the Pt surface. At lower wavenumbers, many bands arise. However, an assignment to specific molecular vibrations is complicated because of the interference of different vibrations to form combinatorial as well as framework vibrations. The comparison with the literature<sup>49,50,51</sup> and theoretical calculations suggest that absorption bands in the region from  $1,158\text{ cm}^{-1}$  to  $1,120\text{ cm}^{-1}$  result from framework vibrations. The band at  $1,063\text{ cm}^{-1}$  as well as the band at  $790\text{ cm}^{-1}$  can be assigned to the amine group. At  $1,063\text{ cm}^{-1}$  the C-N stretch vibration arises while the bands at  $790\text{ cm}^{-1}$  correspond to a combination of wagging and twisting modes of the amine group. Furthermore, the rocking vibration of  $\text{CH}_2$  leads to a characteristic absorption band at  $720\text{ cm}^{-1}$ <sup>49</sup>. Unfortunately, there is no further assignment possible for several bands between  $1,090\text{ cm}^{-1}$  and  $837\text{ cm}^{-1}$ . These bands may result from combinatorial vibrations of the C-C framework. However, such vibrations are not very sensitive to environmental changes, e.g., the vibrations of the amine group and can therefore be neglected.

5-MF shows bands at  $3,124\text{ cm}^{-1}$  and  $2,994\text{ cm}^{-1}$ , which are caused by the C-H stretch vibrations of the ring. The band at  $2,933\text{ cm}^{-1}$  correlates to the C-H stretching vibration of the methyl group<sup>52</sup>. Further bands arise between  $1,211\text{ cm}^{-1}$  and  $800\text{ cm}^{-1}$ . Combinatorial vibrations of the aromatic ring with the methyl group and the C-H in-plane vibration lead to absorption bands at  $1,023\text{ cm}^{-1}$  and  $947\text{ cm}^{-1}$  while the band at  $800\text{ cm}^{-1}$  is assigned to the C-H out-of-plane vibration<sup>52,53</sup>. The bands at  $1,151\text{ cm}^{-1}$  and  $929\text{ cm}^{-1}$  were also observed in the literature for furfural but were not assigned to any vibrational mode<sup>54</sup>.

Investigations on the Pt/DDA nanoparticles reveal that the N-H stretching vibration disappears while the C-H stretching vibrations of the alkyl chain stay mainly unaffected. The disappearance of this band can be explained by the metal surface selection rule, according to which vibrations parallel to the surface cannot be observed. Alternatively, this can also hint toward a breaking of the N-H bond after adsorption on the surface, which would explain the second species in XPS at slightly lower binding energies than the free amine. Another possibility is that the band becomes potentially weaker due to adsorption site constraints and therefore may not be detected due to a bad signal-to-noise ratio. Similarly, the weaker bands in the fingerprint region cannot be observed either.

After ligand exchange of the Pt/DDA nanoparticles with 5-MF under reaction conditions, the wavenumber region above  $2,500\text{ cm}^{-1}$  may exhibit two very weak bands at  $2,924\text{ cm}^{-1}$  and  $2,851\text{ cm}^{-1}$ , which would match to vibration modes of DDA. Additional bands corresponding to 5-MF arise at  $1,101\text{ cm}^{-1}$ ,  $1,053\text{ cm}^{-1}$ ,  $1,022\text{ cm}^{-1}$ ,  $955\text{ cm}^{-1}$ ,  $819\text{ cm}^{-1}$ , and  $798\text{ cm}^{-1}$ . The significant difference between the spectra before and after the addition of 5-MF further enforces the earlier findings of an exchange of DDA with 5-MF. The intensity decreases of the previously strong absorption bands of 5-MF, as well as the strong changes of the vibrations involving the in-plane C-H vibration of the ring ( $3,124\text{ cm}^{-1}$ ,  $2,994\text{ cm}^{-1}$ ,  $1,023\text{ cm}^{-1}$ , and  $947\text{ cm}^{-1}$ ) can be explained by an adsorption geometry of the aromatic ring nearly parallel to the surface and related metal surface selection rules.

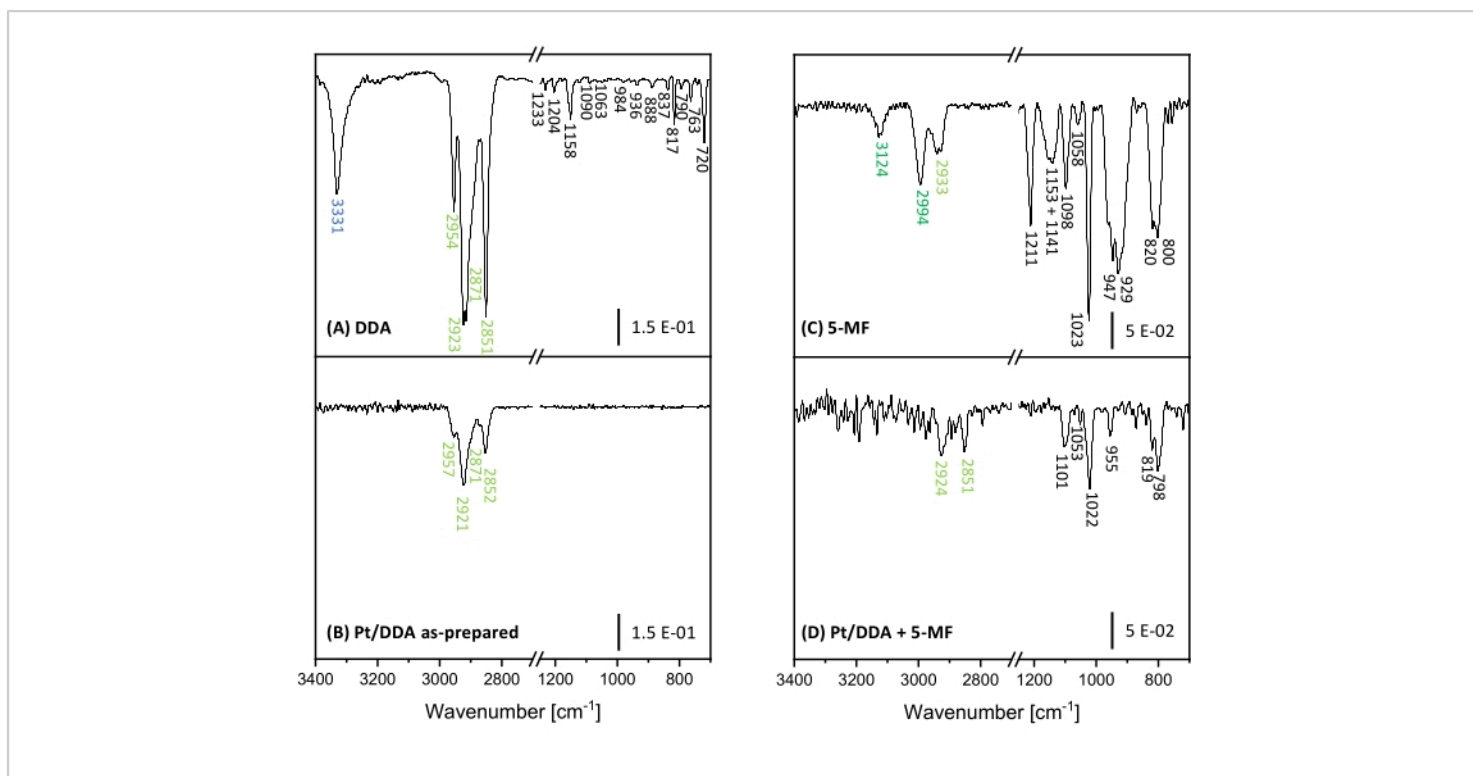


**Figure 7: FT-IR spectra of Pt nanoparticles and references for proof of poisoning.** Shown are the FT-IR spectra of DDA (A) and Pt/DDA nanoparticles (1.3 nm) (B) on the left side. Pure 5-MF (C) and Pt/DDA nanoparticles, which were handled under reaction conditions with pure 5-MF (D) are shown on the right side. [Please click here to view a larger version of this figure.](#)

**Supplementary Table S1: Heating media for hydrogenation reactions.** Listed are the boiling points of different heating media. Diisopropyl ether was used for the hydrogenation of cyclohexene. Since 5-MF did not show any conversion at 69 °C, heating media with higher boiling points were tested. [Please click here to download this Table.](#)

**Supplementary Figure S1: Gas chromatogram of toluene hydrogenation test.** The gas chromatogram shows toluene, which was handled under reaction conditions under 1 atm hydrogen at 69 °C with Pt/DDA/P25 (1.6 nm) as catalyst. This test examined a possible hydrogenation of toluene. A sample was taken after 60 min. No hydrogenation of the solvent could be observed under reaction conditions.

Contaminations are marked with \* and are present in toluene (see **Supplementary Figure S2**). [Please click here to download this File.](#)

**Supplementary Table S2: Retention times of toluene and contaminations in the gas chromatogram for the hydrogenation test.** The sample was taken at 69 °C after 60 min reaction time with Pt/DDA/P25 (1.6 nm) as catalyst. The sampling was carried out with a 1 mL syringe through a septum. Contaminations are marked with \* and are present in toluene (see **Supplementary Figure S2**). [Please click here to download this Table.](#)

**Supplementary Figure S2: Gas chromatogram of toluene.**

The gas chromatogram shows toluene, which has been checked for possible contaminations. Contaminations are marked with \* and were also present in further gas chromatograms. [Please click here to download this File.](#)

**Supplementary Table S3: Retention times of toluene and contaminations in the gas chromatogram for toluene.**

A sample of toluene was taken from the storage container and checked for possible contaminations. Contaminations are marked with \* and are present in toluene (see **Supplementary Figure S2**). [Please click here to download this Table.](#)

**Supplementary Figure S3: Gas chromatogram for hydrogenation of 5-MF after 60 min.**

The sample was taken at 69 °C after 60 min reaction time with Pt/DDA/P25 (1.6 nm) as catalyst. The sampling was carried out with a 1 mL syringe through a septum. [Please click here to download this File.](#)

**Supplementary Table S4: Retention times of substances in the gas chromatogram for the hydrogenation of 5-MF.**

The sample was taken at 69 °C after 60 min reaction time with Pt/DDA/P25 (1.6 nm) as catalyst. [Please click here to download this Table.](#)

**Supplementary Figure S4: Gas chromatogram of possible products.**

This sample contains possible products and by-products for the hydrogenation of 5-methylfurfural in toluene. Contaminations are marked with \* and are present in toluene (see **Supplementary Figure S2**). [Please click here to download this File.](#)

**Supplementary Table S5: Retention times of possible products.**

This table contains possible products and by-products for the hydrogenation of 5-methylfurfural in toluene. Contaminations are marked with \* and are present in toluene

(see **Supplementary Figure S2**). [Please click here to download this Table.](#)

**Supplementary Figure S5: Cutout of the survey spectrum of titania (P25).**

Only one part of the survey of pure titania (P25) is shown, in which the peaks of impurities are located. The impurities result from titania production or the cleaning up process in the industry<sup>44</sup>. The spectrum was measured with Al K $\alpha$  (monochromatic) radiation source (pass energy: 200 eV, energy step size: 1 eV and number of scans: 2) This spectrum is not referenced. [Please click here to download this File.](#)

**Supplementary Figure S6: TEM images and size histograms of amine-stabilized platinum nanoparticles before and after hydrogenation of 5-methylfurfural.**

Shown are the TEM images (at the top) and the size histograms (at the bottom). The left TEM image shows platinum nanoparticles (Pt/DDA/P25 (1.6 nm)) before hydrogenation. The right TEM image shows the platinum nanoparticles (Pt/DDA/P25 (1.6 nm)) after hydrogenation. TEM images were recorded using an acceleration voltage of 80 eV. [Please click here to download this File.](#)

**Supplementary Table S6: Vibrational modes of FT-IR spectra of DDA and Pt/DDA nanoparticles.**

Listed are all bands, which were observed in both measurements and shown in **Figure 7**. Absorption bands that could not be assigned to any vibrational mode are marked with a dash sign (-). [Please click here to download this Table.](#)

**Supplementary Table S7: Vibrational modes of FT-IR spectra of 5-MF and Pt/5-MF nanoparticles.**

Listed are all bands, which were observed in both measurements and shown in **Figure 7**. Absorption bands that could not be

assigned to any vibrational mode are marked with a dash sign (-). [Please click here to download this Table.](#)

## Discussion

Pt nanoparticles capped with DDA were successfully synthesized in two different sizes and shapes<sup>12, 14</sup>. The small Pt nanoparticles (1.6 nm) show a quasi-spherical form while the bigger particles (2.4 nm) are more asymmetrical exhibiting partly tripodal or ellipsoidal structures. The possibilities are limited to gain larger quasi-spherical platinum nanoparticles, since a formation of elongated structures occurs by further increasing the size of the particles by seeded growth<sup>14</sup>. The size and shape of the particles can also be influenced by the ligand, reaction time, and temperature. Besides DDA, other ligands can be used in the synthesis, but the capping agent influences the growth and, therefore, the size and shape of the nanoparticles, as has already been shown for the synthesis of gold nanoparticles<sup>39</sup>. After adding the reduction solution to the metal salt solution, the solution is stirred for 60 min (90 min for the synthesis of larger particles) to ensure that the growth process of the Pt nanoparticles is completed. The transport of monomers to the particle surface can be a limiting factor. Furthermore, the temperature can influence the critical radius, which describes the minimal required particle size, at which seeds are stable in solution. By increasing the temperature, the critical radius decreases, resulting in a faster formation of seeds and consequently a faster decrease of the monomer concentration<sup>55</sup>. After synthesis, ammonium and bromide impurities can still be observed in XPS which can be eliminated by performing a ligand exchange with DDA. Furthermore, all synthesized nanoparticles were deposited on P25 powders without any changes in form, size, or loss of the ligand. For comparison, a ligand-free Pt catalyst was generated by using the impregnation method, which exhibits

a Pt nanoparticle size of 2.1 nm and a quasi-spherical shape. XPS further reveals that not only metallic Pt species were present on the surface but also oxidized species. This indicates that in the absence of amine ligands the platinum nanoparticles interact with the support, which may result in a partial encapsulation of the metal into the support<sup>10</sup>. As a consequence, the particles partially lose their ability to split hydrogen<sup>56</sup>. However, such encapsulation is favored by high temperature reduction of the metal salt precursor. The temperature used here for the reduction (180 °C) is far below those mentioned in the literature for encapsulation (600 °C)<sup>57</sup>. Another more likely explanation would be an incomplete reduction of the used Pt source. However, both explanations result in a partial deactivation of the catalyst.

In literature ligands such as amines or ammonia are often considered as catalyst poison in the classical understanding of heterogeneous catalysis<sup>15, 16</sup>. However, the investigations on the liquid phase hydrogenation of cyclohexene demonstrate that Pt/DDA/P25 is still catalytically active and showed an even higher conversion compared to the amine-free catalyst. Amines are known to systematically block terrace adsorption sites on Pt(111)<sup>11, 58</sup>. Results in the literature have already shown, that this promising active site selecting effect of ligands can be used to improve the selectivity for the hydrogenation of acetylene in ethylene-rich streams by diluting the adsorption sites<sup>59</sup>. This active site selecting effect was also observed for thiols binding on Pd(111)<sup>22, 23</sup>. For the hydrogenation of cyclohexene, these sites are thereby already blocked by amines, however, highly active undercoordinated reaction centers are still available. In addition to the site selection effect of the ligand, attention should also be paid to other properties of the ligand. When selecting the ligand, care should be taken to ensure that the ligand stabilizes the particles

during synthesis and protects them from agglomeration. Furthermore, the ligand should exhibit a strong adsorption on the metal surface and a sufficiently high thermal stability so that the ligand is not desorbed or decomposed under reaction conditions. Results show, that DDA generally seems to be suitable for this catalytic approach. No size effect could be observed in the model reaction. Interestingly, the catalyst containing Pt nanoparticles that did not undergo a ligand exchange exhibited a lower conversion (50%) than Pt particles deposited on P25 after ligand exchange (72%). Therefore, a blocking of active sites by ionic compounds may have to be considered under these conditions. Performing a ligand exchange is crucial to increase the activity of the platinum nanoparticles by removing co-adsorbed ionic compounds such as bromide and ammonium, as XPS before and after ligand exchange shows.

Additionally, the influence of the extra amine surface species on the catalytic activity of platinum nanoparticles remains ambiguous, as this species can potentially serve as an additional, localized hydrogen source. XP spectra and FT-IR spectra seem to indicate a hydrogen abstraction of the amine group by platinum leading to an extra amine surface species. This offers the opportunity to serve hydrogen additionally to the dissolved hydrogen in toluene, which can affect the catalytic activity. A hydrogen donor effect from toluene can be excluded here since toluene is not known to dehydrogenate under low hydrogen pressure and temperature<sup>60</sup>. However, the influence of hydrogen abstraction on the catalytic activity still needs to be further investigated. The hydrogenation of acetophenone on l-proline-modified platinum nanoparticles has already shown that the amine group can accelerate the hydrogenation by a hydrogen transfer from the amine to the reactant<sup>15</sup>. Therefore, a possible influence of the amine

and the surface species on the hydrogenation should be considered.

Despite the successful use of Pt/DDA nanoparticles for the hydrogenation of simple alkenes, no turnover for the more demanding reactant 5-MF could be observed. Therefore, different possibilities for this may be discussed in the following: one explanation would be that no reaction takes place because of the low reaction temperature and hydrogen pressure. The reaction temperature was limited to 160 °C. As thermogravimetric analysis showed ligand desorption and decomposition of Pt/DDA nanoparticles of comparable sizes take place at these temperatures<sup>13</sup>. Due to the used reactor, no higher pressures than 1 atm of hydrogen could be used. The lower hydrogen pressure in contrast to literature experiments might be the reason why the hydrogenation of carbonyl compounds, such as 5-MF, was not feasible. Several studies have further shown that strong metal support interactions (SMSI) are crucial for the selectivity of the gas-phase hydrogenation of furfural<sup>61,62,63</sup>. The SMSI leads to the formation of O-vacancies, which enables the adsorption of furfural *via* the carbonyl group on the titania surface. A furfuryl-oxy-intermediate is formed that can be hydrogenated. However, this hypothesis is countered by the fact that, in contrast to the gas phase experiments, no evidence for an influence of SMSI could be found for liquid phase hydrogenation of furfural in methanol. Platinum particles on different oxides (MgO, CeO<sub>2</sub>, and Al<sub>2</sub>O<sub>3</sub>) had shown comparable catalytic properties<sup>64</sup>. This indicates that the hydrogenation could take place undergoing different mechanisms in the liquid and gas phase, which needs to be further investigated. The SMSI effect of the Pt particles and the support were only observed for the ligand-free catalyst, which also does not show any conversion of 5-MF under the used reaction conditions. Therefore an impact of the SMSI

effect seems unlikely. As poisoning of the catalyst by 5-MF or a surface intermediate seems more probable under the applied reaction conditions, the catalysts were further analyzed before and after ligand exchange with 5-MF under reaction conditions by XPS and FT-IR. These measurements confirmed the hypothesis of catalyst poisoning by 5-MF as both methods show a decrease in the peaks corresponding

to the amine on the Pt surface. FT-IR spectroscopy further hints that 5-MF acts as catalyst poison since bands appear in the wavenumber region below  $1,200\text{ cm}^{-1}$ , which are consistent with the bands assigned to 5-MF. A nearly flat adsorption geometry is suggested taking surface selections rules into account. A schematic drawing for the proposed surface restructuring is shown in **Figure 8**.

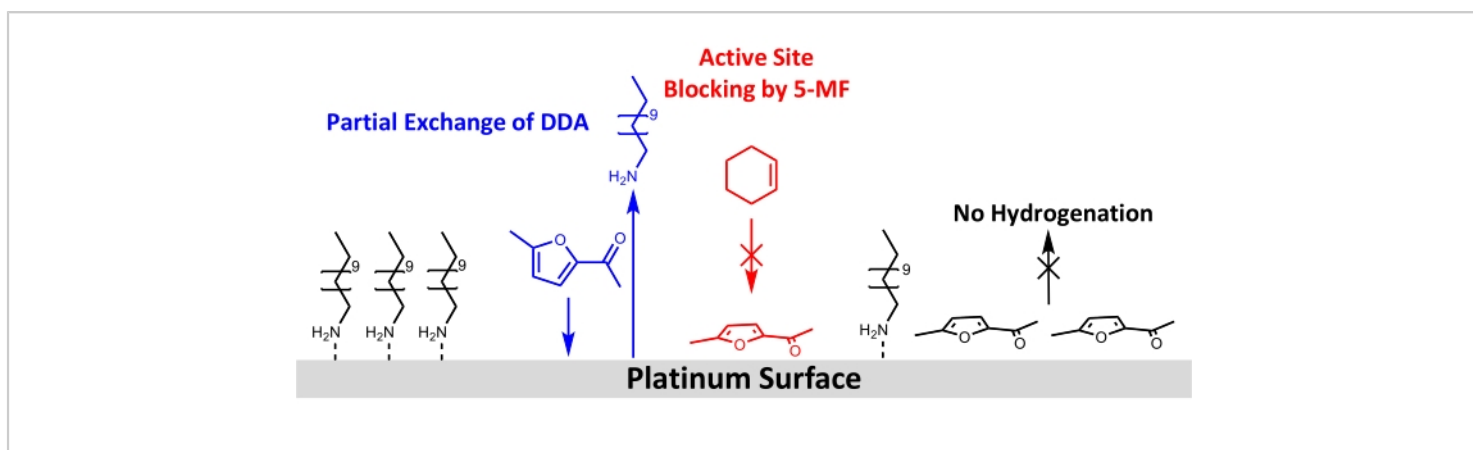


**Figure 8: Schematic drawing of structural changes by adding 5-MF to the hydrogenation of cyclohexene at the surface of amine-stabilized platinum nanoparticles.** Results from FT-IR and XPS show a partial exchange of DDA by 5-MF at the platinum surface and blocking of active sites for the hydrogenation of cyclohexene. Results of FT-IR data suggest an adsorption of the ring of 5-MF nearly parallel to the surface. [Please click here to view a larger version of this figure.](#)

To conclude, amine-capped Pt nanoparticles on P25 are promising candidates for new hydrogenation catalysts as the Pt nanoparticles show a higher conversion than the ligand-free catalyst in the model reaction. However, no conversion of 5-MF was observed on either catalyst. This results from poisoning of the Pt by the reactant and not by the ligand as often considered in the literature under the investigated reaction conditions. For future applications, further understanding of the influence of ligands on the adsorption behavior of reactants and their interaction with metal nanoparticles are needed. A colloidal synthesis is a promising approach besides

impregnation and calcination methods for the fabrication of heterogeneous catalysts, as this allows the synthesis of nanoparticles in defined size and shape. Since the colloidal synthesis approach allows the use of different ligands, for instance, amines, amides, thiols, or alcohols, Pt nanoparticles with other ligands should be investigated and compared. This offers the possibility to use ligands, which show a specific ligand-reactant interaction, such as  $\pi$ - $\pi$  interactions to control the adsorption geometry and thus also the selectivity of the reaction. This approach could be used for the selective hydrogenation of  $\alpha,\beta$ -unsaturated ketones and aldehydes, as has already been shown

for the hydrogenation of cinnamaldehyde<sup>21</sup>. Furthermore, controlling the stereoselectivity in heterogeneous catalyzed reactions is still a challenging task; however, an appropriate chiral ligand could be used to control the chirality of the product as in homogeneous catalyzed reactions. Besides the ligand-reactant interactions, the stabilizing effect of ligands might be used for protecting metal nanoparticles from strong metal support interaction. The strong metal support interaction would lower the chemisorption of hydrogen by encapsulation of the particles with an oxide layer. For a better understanding of the influence of ligands, XPS and FT-IR can provide useful information about the selective poisoning effect and the binding modes of ligands. Furthermore, CO shall be considered as a sensor molecule to identify available surface sites of the Pt nanoparticle. Additionally, the adsorption behavior and possible surface reactions of ligands and reactants can be investigated on Pt single crystals under ultra-high vacuum conditions to get a fundamental understanding of the surface processes. All in all, ligands in heterogeneous catalysis can offer a new catalytic approach, which can be used to control the activity and selectivity of a catalyzed reaction besides the particle size and support effects. Therefore, the traditional way of thinking for heterogeneous catalysis of ligands as catalyst poison should be reconsidered.

## Disclosures

The authors have nothing to disclose.

## Acknowledgments

Thanks go to Edith Kieselhorst and Erhard Rhiel for support at the TEM and to Carsten Dosche for support at the XPS. Thanks to Stefan Petrasz for support with the gas

chromatograph. The funding of the XPS device by DFG (INST: 184/144-1FUGG) and funding from DFG-RTG 2226 is acknowledged.

## References

1. Liu, L., Corma, A. Metal catalysts for heterogeneous catalysis: From single atoms to nanoclusters and nanoparticles. *Chemical Reviews*. **118** (10), 4981-5079 (2018).
2. Zakarina, N., Bekturov, E. Platinum nanoparticles stabilized by polyvinylpyrrolidone for hydrogenation. *Chinese Journal of Catalysis*. **29** (11), 1165-1168 (2008).
3. Rioux, R. M. et al. Monodisperse platinum nanoparticles of well-defined shape: synthesis, characterization, catalytic properties and future prospects. *Topics in Catalysis*. **39** (3-4), 167-174 (2006).
4. Ikeda, S. et al. Ligand-free platinum nanoparticles encapsulated in a hollow porous carbon shell as a highly active heterogeneous hydrogenation catalyst. *Angewandte Chemie*. **118** (42), 7221-7224 (2006).
5. Mostafa, S. et al. Shape-dependent catalytic properties of Pt nanoparticles. *Journal of the American Chemical Society*. **132** (44), 15714-15719 (2010).
6. van Deelen, T. W., Hernández Mejía, C., Jong, K. P. Control of metal-support interactions in heterogeneous catalysts to enhance activity and selectivity. *Nature Catalysis*. **2** (11), 955-970 (2019).
7. Rioux, R. M., Hsu, B. B., Grass, M. E., Song, H., Somorjai, G. A. Influence of particle size on reaction selectivity in cyclohexene hydrogenation and dehydrogenation over silica-supported monodisperse Pt particles. *Catalysis Letters*. **126** (1-2), 10-19 (2008).

8. Somorjai, G. A., Carrazza, J. Structure sensitivity of catalytic reactions. *Industrial & Engineering Chemistry Fundamentals*. **25** (1), 63-69 (1986).
9. Somorjai, G. A. Surface science. *Science (New York, N.Y.)*. **201** (4355), 489-497 (1978).
10. Fu, Q., Wagner, T. Interaction of nanostructured metal overlayers with oxide surfaces. *Surface Science Reports*. **62** (11), 431-498 (2007).
11. Siemer, M., Tomaschun, G., Klüner, T., Christopher, P., Al-Shamery, K. Insights into spectator-directed catalysis: CO adsorption on amine-capped platinum nanoparticles on oxide supports. *ACS Applied Materials & Interfaces*. **12** (24), 27765-27776 (2020).
12. Jana, N. R., Peng, X. Single-phase and gram-scale routes toward nearly monodisperse Au and other noble metal nanocrystals. *Journal of the American Chemical Society*. **125** (47), 14280-14281 (2003).
13. Fenske, D. et al. Colloidal synthesis of Pt nanoparticles: on the formation and stability of nanowires. *Langmuir*. **24** (16), 9011-9016 (2008).
14. Osmić, M., Kolny-Olesiak, J., Al-Shamery, K. Size control and shape evolution of single-twinned platinum nanocrystals in a room temperature colloidal synthesis. *CrystEngComm*. **16** (42), 9907-9914 (2014).
15. Schrader, I., Warneke, J., Backenköhler, J., Kunz, S. Functionalization of platinum nanoparticles with L-proline: simultaneous enhancements of catalytic activity and selectivity. *Journal of the American Chemical Society*. **137** (2), 905-912 (2015).
16. Maxted, E. B., Biggs, M. S. The catalytic toxicity of nitrogen compounds. Toxicity of ammonia and of amines. *Journal of the Chemical Society*. 3844-3847 (1957).
17. Aliaga, C. et al. Sum frequency generation and catalytic reaction studies of the removal of organic capping agents from Pt nanoparticles by UV-Ozone treatment. *The Journal of Physical Chemistry C*. **113** (15), 6150-6155 (2009).
18. Comotti, M., Li, W.-C., Spliethoff, B., Schüth, F. Support effect in high activity gold catalysts for CO oxidation. *Journal of the American Chemical Society*. **128** (3), 917-924 (2006).
19. Gorin, D. J., Sherry, B. D., Toste, F. D. Ligand effects in homogeneous Au catalysis. *Chemical Reviews*. **108** (8), 3351-3378 (2008).
20. Kahsar, K. R., Schwartz, D. K., Medlin, J. W. Selective hydrogenation of polyunsaturated fatty acids using alkanethiol self-assembled monolayer-coated Pd/Al<sub>2</sub>O<sub>3</sub> catalysts. *ACS Catalysis*. **3** (9), 2041-2044 (2013).
21. Kahsar, K. R., Schwartz, D. K., Medlin, J. W. Control of metal catalyst selectivity through specific noncovalent molecular interactions. *Journal of the American Chemical Society*. **136** (1), 520-526 (2014).
22. Pang, S. H., Schoenbaum, C. A., Schwartz, D. K., Medlin, J. W. Directing reaction pathways by catalyst active-site selection using self-assembled monolayers. *Nature Communications*. **4**, 2448 (2013).
23. Schoenbaum, C. A., Schwartz, D. K., Medlin, J. W. Controlling the surface environment of heterogeneous catalysts using self-assembled monolayers. *Accounts of Chemical Research*. **47** (4), 1438-1445 (2014).
24. Grimes, R. N. Small carborane ligands as spectators and as players. *Journal of Organometallic Chemistry*. **581** (1-2), 1-12 (1999).

25. Crabtree, R.H. Multifunctional ligands in transition metal catalysis. *New Journal of Chemistry*. **35** (1), 18-23 (2011).
26. Dostert, K.-H., O'Brien, C. P., Ivars-Barceló, F., Schauermaun, S., Freund, H.-J. Spectators control selectivity in surface chemistry: Acrolein partial hydrogenation over Pd. *Journal of the American Chemical Society*. **137** (42), 13496-13502 (2015).
27. Hu, L. et al. Catalytic conversion of biomass-derived carbohydrates into fuels and chemicals via furanic aldehydes. *RSC Advances*. **2** (30), 11184 (2012).
28. Pushkarev, V. V., Musselwhite, N., An, K., Alayoglu, S., Somorjai, G. A. High structure sensitivity of vapor-phase furfural decarbonylation/hydrogenation reaction network as a function of size and shape of Pt nanoparticles. *Nano Letters*. **12** (10), 5196-5201 (2012).
29. Liao, X.-M., Pitchon, V., Cuong, P.-H., Chu, W., Caps, V. Hydrogenation of cinnamaldehyde over bimetallic Au-Cu/CeO<sub>2</sub> catalyst under a mild condition. *Chinese Chemical Letters*. **28** (2), 293-296 (2017).
30. Fang, D., He, F., Xie, J., Xue, L. Calibration of binding energy positions with C1s for XPS results. *Journal of Wuhan University of Technology-Materials Science Edition*. **35** (4), 711-718 (2020).
31. Heiz, U., Landman, U. *Nanocatalysis: With 14 tables*. Springer. Berlin, Heidelberg (2008).
32. Nyholm, R., Berndtsson, A., Martensson, N. Core level binding energies for the elements Hf to Bi (Z=72-83). *Journal of Physics C: Solid State Physics*. **13** (36), L1091-L1096 (1980).
33. Fu, X., Wang, Y., Wu, N., Gui, L., Tang, Y. Surface modification of small platinum nanoclusters with alkylamine and alkylthiol: An XPS study on the influence of organic ligands on the Pt 4f binding energies of small platinum nanoclusters. *Journal of Colloid and Interface Science*. **243** (2), 326-330 (2001).
34. Ono, L. K., Yuan, B., Heinrich, H., Cuenya, B. R. Formation and thermal stability of platinum oxides on size-selected platinum nanoparticles: Support effects. *The Journal of Physical Chemistry C*. **114** (50), 22119-22133 (2010).
35. Bachmann, P. et al. Dehydrogenation of the Liquid Organic Hydrogen Carrier System Indole/Indoline/Octahydroindole on Pt(111). *The Journal of Physical Chemistry C*. **122** (8), 4470-4479 (2018).
36. Mudiyansele, K., Trenary, M. Adsorption and thermal decomposition of N-methylaniline on Pt(111). *Surface Science*. **603** (21), 3215-3221 (2009).
37. Briggs, D., Beamson, G. Primary and secondary oxygen-induced C1s binding energy shifts in x-ray photoelectron spectroscopy of polymers. *Analytical Chemistry*. **64** (15), 1729-1736 (1992).
38. Huang, M., Adnot, A., Suppiah, S., Kaliaguine, S. XPS observation of surface interaction between H<sub>2</sub> and CO<sub>2</sub> on platinum foil. *Journal of Molecular Catalysis A: Chemical*. **104** (2), L131-L137 (1995).
39. Mohrhusen, L., Osmić, M. Sterical ligand stabilization of nanocrystals versus electrostatic shielding by ionic compounds: a principle model study with TEM and XPS. *RSC Advances*. **7** (21), 12897-12907 (2017).
40. Otero-Irurueta, G. et al. Adsorption and coupling of 4-aminophenol on Pt(111) surfaces. *Surface Science*. **646**, 5-12 (2015).

41. Erley, W., Xu, R., Hemminger, J. C. Thermal decomposition of trimethylamine on Pt(111): spectroscopic identification of surface intermediates. *Surface Science*. **389** (1–3), 272–286 (1997).
42. Bridge, M. E., Somers, J. The adsorption of methylamine on Pt(111). *Vacuum*. **38** (4–5), 317–320 (1988).
43. Chen, X., Mao, S. S. Titanium dioxide nanomaterials: synthesis, properties, modifications, and applications. *Chemical Reviews*. **107** (7), 2891–2959 (2007).
44. Madon, R. J., O'Connell, J. P., Boudart, M. Catalytic hydrogenation of cyclohexene: Part II. Liquid phase reaction on supported platinum in a gradientless slurry reactor. *American Institute of Chemical Engineers Journal*. **24** (5), 904–911 (1978).
45. Pan, C.-J. et al. Tuning/exploiting Strong Metal-Support Interaction (SMSI) in heterogeneous catalysis. *Journal of the Taiwan Institute of Chemical Engineers*. **74**, 154–186 (2017).
46. Lewera, A., Timperman, L., Roguska, A., Alonso-Vante, N. Metal–support interactions between nanosized Pt and metal oxides (WO<sub>3</sub> and TiO<sub>2</sub>) studied using X-ray photoelectron spectroscopy. *The Journal of Physical Chemistry C*. **115** (41), 20153–20159 (2011).
47. Ohyama, J., Yamamoto, A., Teramura, K., Shishido, T., Tanaka, T. Modification of metal nanoparticles with TiO<sub>2</sub> and metal–support interaction in photodeposition. *ACS Catalysis*. **1** (3), 187–192 (2011).
48. Zhong, J.-Q. et al. Synchrotron-based ambient pressure X-ray photoelectron spectroscopy of hydrogen and helium. *Applied Physics Letters*. **112** (9), 91602 (2018).
49. Günzler, H., Gremlich, H.-U. *IR-Spektroskopie: Eine Einführung*. Wiley; WILEY-VCH. Hoboken, NJ, Weinheim (2003).
50. Hesse, M., Meier, H., Zeeh, B. *Spektroskopische Methoden in der organischen Chemie: 114 Tabellen*. Thieme. Stuttgart (2012).
51. Ripmeester, M., Duford, D. A., Yuan, S. Understanding the behaviour of dodecylamine as a model cationic collector in oil sands tailings dewatering applications using a novel FTIR based method. *The Canadian Journal of Chemical Engineering*. **98** (7), 1471-1482 (2020).
52. Erdogdu, Y., Sertbakan, T. R., Güllüoğlu, M. T., Yurdakul, Ş., Güvenir, A. FT-IR and Raman spectroscopy and computation of 5-Methylfurfural. *Journal of Applied Spectroscopy*. **85** (3), 517-525 (2018).
53. Kiss, Á. I., Machytka, D., Bánki, J., Gál, M. Spectroscopic study of the conformational isomerism of 2-formylfuran derivatives. *Journal of Molecular Structure*. **197**, 193-202 (1989).
54. Allen, G., Bernstein, H. J. Internal rotation: VIII. The infrared and Raman spectra of furfural. *Canadian Journal of Chemistry*. **33** (6), 1055-1061 (1955).
55. Thanh, N. T. K., Maclean, N., Mahiddine, S. Mechanisms of nucleation and growth of nanoparticles in solution. *Chemical Reviews*. **114** (15), 7610-7630 (2014).
56. Tauster, S. J., Fung, S. C., Garten, R. L. Strong metal-support interactions. Group 8 noble metals supported on titanium dioxide. *Journal of the American Chemical Society*. **100** (1), 170-175 (1978).
57. Beck, A. et al. The dynamics of overlayer formation on catalyst nanoparticles and strong metal-support interaction. *Nature Communications*. **11** (1), 3220 (2020).

58. Sobota, M. et al. Ligand effects in SCILL model systems: site-specific interactions with Pt and Pd nanoparticles. *Advanced Materials*. **23** (22–23), 2617-2621 (2011).
59. Altmann, L. et al. Impact of organic ligands on the structure and hydrogenation performance of colloiddally prepared bimetallic PtSn nanoparticles. *ChemCatChem*. **5** (7), 1803-1810 (2013).
60. Modisha, P. M., Ouma, C. N. M., Garidzirai, R., Wasserscheid, P., Bessarabov, D. The prospect of hydrogen storage using liquid organic hydrogen carriers. *Energy & Fuels*. **33** (4), 2778-2796 (2019).
61. Baker, L. R. et al. Furfuraldehyde hydrogenation on titanium oxide-supported platinum nanoparticles studied by sum frequency generation vibrational spectroscopy: acid-base catalysis explains the molecular origin of strong metal-support interactions. *Journal of the American Chemical Society*. **134** (34), 14208-14216 (2012).
62. Kijeński, J., Winiarek, P., Paryjczak, T., Lewicki, A., Mikołajska, A. Platinum deposited on monolayer supports in selective hydrogenation of furfural to furfuryl alcohol. *Applied Catalysis A: General*. **233** (1-2), 171-182 (2002).
63. Kijeński, J., Winiarek, P. Selective hydrogenation of  $\alpha,\beta$ -unsaturated aldehydes over Pt catalysts deposited on monolayer supports. *Applied Catalysis A: General*. **193** (1-2), L1-L4 (2000).
64. Taylor, M. J. et al. Highly selective hydrogenation of furfural over supported Pt nanoparticles under mild conditions. *Applied Catalysis B*. **180**, 580-585 (2016).